RESEARCH PAPER

Effect of Heat Treatment on the Microstructure and Soft Magnetic Properties of the Amorphous Fe-B-P-Cu Alloy

S. Mirzaei[1], H. Saghafian[1,*], A. Beitollahi[1], J. Świerczek[2] and P. Tiberto[3]

**saghafian@iust.ac.ir*

Received: April 2018 **Revised: August 2018** **Accepted: October 2018**

[1] School of Metallurgy and Materials Engineering, Iran University of Science and Technology, Tehran, Iran.

[2] Institute of Physics, Częstochowa University of Technology, 42-200 Częstochowa, Poland

[3] INRIM, Electromagnetism Division, Strada delle Cacce 91, Torino, Italy.

DOI: 10.22068/ijmse.16.2.1

Abstract: *In the present research, rapidly solidified $Fe_{85.3}B_{11}P_3Cu_{0.7}$ ribbons were prepared by melt spinning process. The microstructural variation, as well as magnetic properties of the as-spun and annealed ribbons, were characterized by X-ray diffraction (XRD), transmission Mossbauer spectroscopy and alternating gradient field magnetometer (AGFM). The results showed two separated distinct exothermic peaks during heating, resulting from the phase transition from amorphous to α-Fe and then to Fe_3B, respectively. The study of magnetic properties in the amorphous and nanocrystalline states revealed that annealing the amorphous ribbons at 440˚C for 10 minutes gives rise to a significant increase in saturation magnetization (220 emu/g) which makes this alloy a good candidate for power applications.*

Keywords: *Melt spinning, Mossbauer spectroscopy, Crystallization, Soft magnetic properties.*

1. INTRODUCTION

During the last decades, Fe-based amorphous and nanocrystalline soft magnetic alloys, such as FeSiBCuNb [1], FeSiBCu [2] and FeSiBPCu [3] have attracted great attention due to their ability to attain excellent soft magnetic properties such as high saturation magnetization (M_s), low coercivity (H_c) and low magnetic core loss [4]. Furthermore, the structural evolution of the amorphous alloys during the crystallization process is of high interest for the purpose of obtaining nanocrystalline materials with excellent soft magnetic properties [4]. Nanocrystalline alloys are mostly fabricated by partial crystallization of amorphous precursors, giving rise to the formation of ferromagnetic nanocrystals surrounded by residual amorphous phase [5].

Heating the amorphous ribbons at temperatures higher than the first crystallization temperature gives rise to the transformation of amorphous precursors into a composite structure consisting of α-Fe nanograins embedded in an amorphous matrix [4]. It has been shown [6] that the increase of Fe content could reduce the cost of alloys and improve magnetic properties. The addition of the B element can control the grain size because it stabilizes the residual amorphous phase and hence prevents further grain growth [6]. Makino et al. [3, 7] reported that by simultaneous addition of Cu and P, separation of small region enriched with Cu and P occurs in the amorphous phase. These regions can act as heterogeneous nucleation sites for α-Fe grains and promote grain refinement [3, 7].

In the present work, Mossbauer spectra and the deduced magnetic hyperfine field distributions together with the changes in the microscopic state of iron atoms in $Fe_{85.3}B_{11}P_3Cu_{0.7}$ ribbons in amorphous and nanocrystalline states were analyzed to clarify the mechanism of the crystallization process. Furthermore, the effect of the primary and secondary crystallization on the soft magnetic properties of rapidly solidified ribbons was investigated.

2. EXPERIMENTAL PROCEDURE

The alloy ingot with a nominal composition of $Fe_{85.3}B_{11}P_3Cu_{0.7}$ was produced by arc melting using high purity elements Fe, B, Cu and pre-alloyed Fe_3P in a vacuum. The as-quenched ribbons with

[DOI: 10.22068/ijmse.16.3.1]

a width of 0.6 mm and a thickness of 16 μm were prepared by single roller melt spinning method under a high-purity argon atmosphere onto a rotating copper wheel with a surface velocity of 40 m/s. The melt-spun ribbons were found to be fully ductile. The initial as-quenched state and the annealed structures were examined by a PANalytical X'Pert PRO MPD X-ray diffractometer (XRD) with Cu Kα radiation and a room-temperature POLON type transmission Mossbauer spectrometer using a conventional constant acceleration spectrometer with a ^{57}Co(Rh) radioactive source. The spectrometer was calibrated and the isomer shift was determined with respect to the alpha-Fe polycrystalline foil. Spectra were fitted by means of the NORMOS package written by R.A. Brand [8].

The thermal properties of melt-spun ribbons were evaluated with a Mettler Toledo differential scanning calorimeter (DSC) under an N_2 gas flow at a heating rate of 10 ˚C/min. To study the changes of microstructure and magnetic properties in the $Fe_{85.3}B_{11}P_3Cu_{0.7}$ alloy, the as-spun ribbons were encapsulated in the vacuum and annealed at various temperatures. The annealing temperatures for the ribbons were decided based on the crystallization temperature obtained from the DSC curves. Annealing was carried out by keeping the as-quenched ribbons for 10 minutes in the tubular furnace preheated at 440, 530 and 650 ˚C in advance. Room temperature magnetization measurements have been performed with a PRINCETON alternating gradient field magnetometer (AGFM) with a maximum magnetizing field of 19 kOe.

3. RESULTS AND DISCUSSION

3.1. Structural Analysis

The X-ray diffraction patterns taken from both sides of the rapidly quenched $Fe_{85.3}B_{11}P_3Cu_{0.7}$ ribbons are shown in Fig. 1. As can be seen in this figure, only a broad amorphous halo is observed on the air side of the as-spun ribbons. Whereas, besides this broad amorphous halo on the wheel side, there is a sharp crystallization peak, close to the (200) α-Fe diffraction. These results indicate that the α-Fe crystalline phase is probably present on both sides of the rapidly quenched ribbons. Kraus et al. [9] in a similar study reported the crystallites were concentrated close to the surface of the wheel side, whereas on the air side they were extended much deeper along with ribbon thickness [9]. This can be ascribed to the large density of defects (air pockets) on the wheel side which facilitates the nucleation of α-Fe crystalline phase on this side with respect to the air side.

Air pockets exist on the wheel side of the melt-spun ribbons and originate from the air entrapment during the melt spinning process [10] (Fig. 2). During the production of ribbons, on the air side of the ribbon the air ejects to the outside while in the case of wheel side of the ribbon, due to the high speed of the wheel, air can be entrapped between wheel surface and the ribbon [10]. This gives rise to the creation of air pockets on the wheel side of the ribbons according to Vishwanadh et al [10].

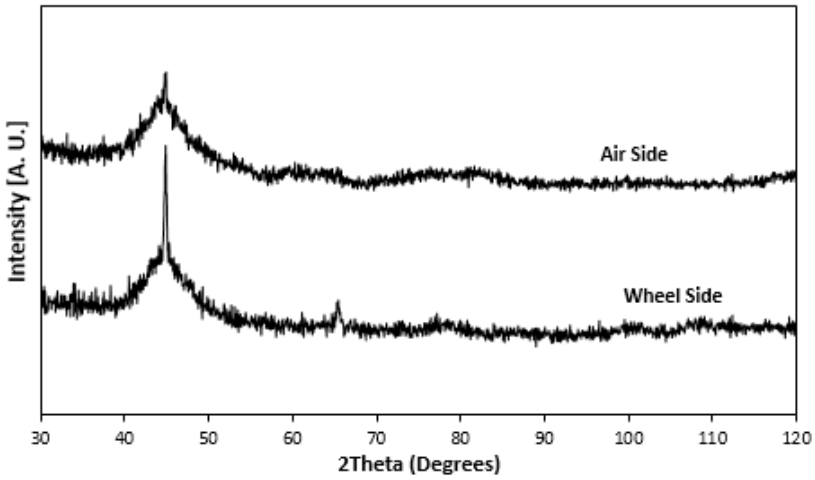

Fig. 1. X-ray diffraction patterns for air- and wheel-side of as-spun $Fe_{85.3}B_{11}P_3Cu_{0.7}$ ribbon.

[DOI: 10.22068/ijmse.16.3.1]

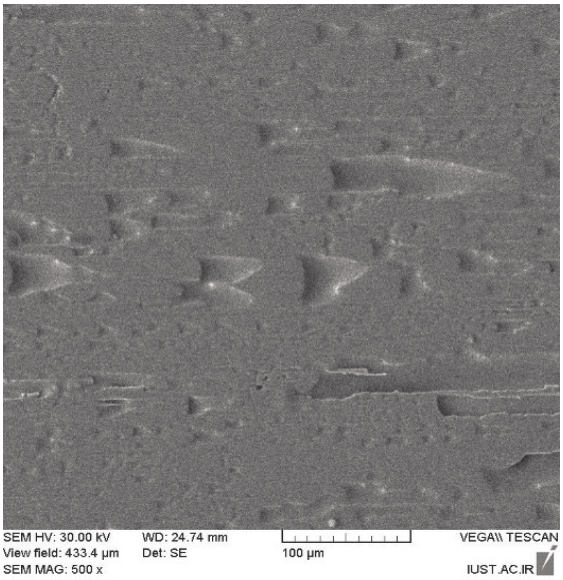

Fig. 2. SEM micrograph of the wheel side of $Fe_{85.3}B_{11}P_3Cu_{0.7}$ ribbon, showing air pockets.

In order to study the structure of the as-spun $Fe_{85.3}B_{11}P_3Cu_{0.7}$ ribbons more precisely, transmission Mossbauer spectroscopy was utilized. A Mossbauer spectrum presents quantitative data on hyperfine interactions which are small energies from the interaction between the nucleus and its surrounding electrons [11]. In fact, Mossbauer spectroscopy makes a quantitative evaluation of the local structure and local composition variations possible [12]. So, it can be used as a detailed probe of the Fe neighborhood to check the crystallization progress during the annealing.

Room temperature transmission Mossbauer spectrum of the as-spun ribbons and the corresponding hyperfine field distribution for the parent amorphous alloy are presented in Fig. 3. The spectrum is asymmetrical and consists of wide, overlapping lines which is typical for amorphous alloys [13]. In the hyperfine field distribution, two components are distinguishable: low-field component (at about 12T) and high-field component (at about 25T).

The presence of two separated components can be attributed to the presence of two different iron atom surroundings [14]. Low field component can be associated with those Fe atoms which have primarily Cu and B as nearest neighbors [14], whereas the high field component is ascribed to the Fe atoms surrounded by Fe and B atoms.

The best fitted hyperfine parameters are listed in Table 1. In this table B_{hf} is the average value of the hyperfine field induction distribution, ΔB_{hf} is its standard deviation, a and b are parameters of the relation $IS=aB_{hf}+b$, IS is the average value of the isomer shift, $I_{2,5}$ is the relative intensity of the second and fifth lines and A is the relative subspectrum area.

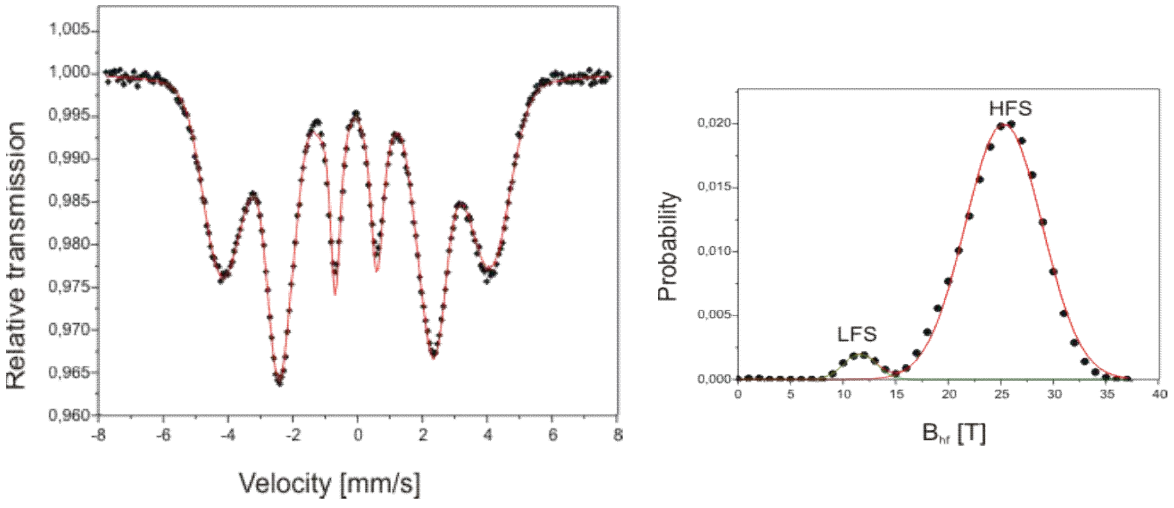

Fig. 3. Room temperature transmission Mossbauer spectrum (a) and corresponding hyperfine field distribution (b) of the as-spun $Fe_{85.3}B_{11}P_3Cu_{0.7}$ ribbons.

[DOI: 10.22068/ijmse.16.3.1]

Table 1. Best fitted hyperfine parameters for the as-spun $Fe_{85.3}B_{11}P_3Cu_{0.7}$ ribbon.

Sample	[T]$\overline{B_{hf}}$	Δ B_{hf} [T]	a [mm/(sT)]	b [mm/s]	$\overline{IS}$[mm/s]	$I_{2,5}$(2,5)	*A*[%]
as-spun	24.50	4.43	0.0052	-0.180	0.052	2.82	100

The obtained results confirm the achievement of the amorphous structure for the rapidly solidified ribbons. However, it should be noted that transmission Mossbauer spectroscopy gives the information from the volume of the sample. To study the partially crystallized surface layer, which is formed during the melt spinning process, conversion electron Mossbauer spectroscopy (CEMS) should be used.

The annealing temperatures to obtain nanocrystalline structure were determined using non-isothermal differential scanning calorimetry (DSC). Non-isothermal DSC curves of melt spun $Fe_{85.3}B_{11}P_3Cu_{0.7}$ amorphous ribbon at heating rates of 10 and 20˚C/min are presented in Fig. 4. It can be seen that the temperatures of primary and secondary crystallization are well separated.

Based on the results from the DSC curve, the ribbons were annealed at 440, 530 and 650˚C for 10 minutes and the corresponding XRD patterns are reported in Fig. 5. As can be understood from this figure, heating the amorphous ribbons for 10 minutes at 440˚C gives rise to the formation of α-Fe phase. Makino et al. [3] have also reported that for the Fe-Si-B-P-Cu alloys with high Fe content, due to the positive mixing enthalpy between Fe and Cu atoms (+13 kJ/mol) and the negative one between Cu and P atoms (-9 kJ/mol), there are repulsive and attractive interactions between Fe, Cu and Cu, P atoms, respectively. As a result, very small regions enriched with Cu and P atoms could separate from the amorphous phase and probably act as nucleation sites for α-Fe grains [3].

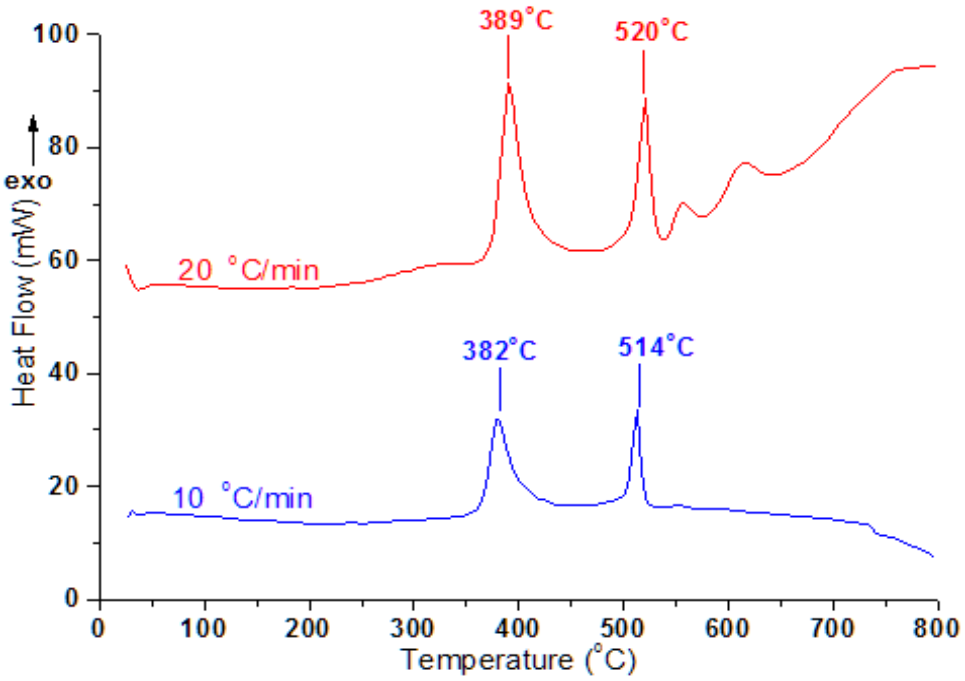

Fig. 4. DSC curves of melt spun $Fe_{85.3}B_{11}P_3Cu_{0.7}$ amorphous ribbons obtained at heating rates of 10, 20˚C/min.

[DOI: 10.22068/ijmse.16.3.1]

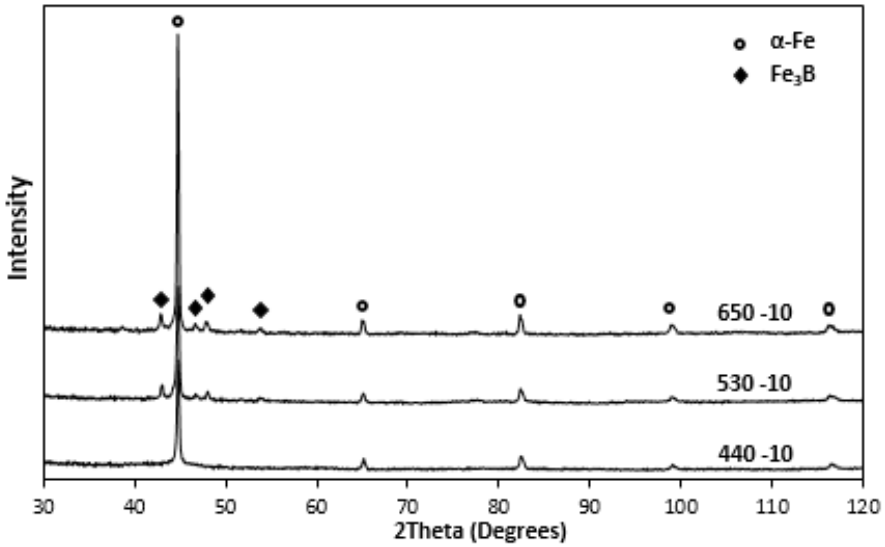

Fig. 5. XRD patterns of $Fe_{85.3}B_{11}P_3Cu_{0.7}$ ribbons annealed at 440, 530 and 650˚C for 10 minutes.

Jafari et al. [15] have demonstrated that during the annealing of $Fe_{84.3}Si_4B_8P_3Cu_{0.7}$ ribbons, boron and phosphorous atoms are rejected from α-Fe(Si) phase and enriched in the residual amorphous matrix. They showed that Cu clusters were distributed homogenously in contact with α-Fe(Si) nanocrystals [15]. This indicates that Cu clusters act as heterogeneous nucleation sites for α-Fe(Si) crystallization [15].

With increasing annealing temperature to 530 ˚C, Fe_3B was formed, as well. The formation of iron boride phases during the second stage of crystallization have been also reported for Fe-Cu-Nb-Si-B [16], Fe-Co-Si-B-Nb-Cu-Ni [17] and Fe-Si-B-Nb-Cu-Ni [18] alloys. As can be understood from Fig. 5, no new phase can be formed with a further increase in temperature up to 650˚C. The calculation of crystallite size using Scherer equation revealed no significant increase in α-Fe crystallite size from 440 ˚C (40 nm) to 530 ˚C (39 nm), whereas a fast increment of the crystallite size was observed at 650 ˚C (66 nm). This may be interpreted that the presence of the residual amorphous matrix can hinder the grain growth to some extent.

The microstructural evaluation of the as-spun ribbons during the crystallization process was conducted using Mossbauer spectroscopy. The spectrum of the sample annealed at 440 ˚C for 10 minutes (Fig. 6a) was best fitted with two subspectra; one subspectrum with a hyperfine field of about 33T corresponds to the α-Fe phase which is compatible with XRD results and the reported values by other researchers [19, 20]. The other subspectrum with an average hyperfine field of about 24.9 T is attributed to the residual amorphous phase with the magnetic hyperfine field induction distribution shown in Fig. 6b. The hyperfine field distribution function $P(B_{hf})$ can be presented as a sum of four Gaussian distributions G1, G2, G3 and G4 centered at 10.04, 20.84, 24.82 and 30.09 T, respectively (Fig.6b). The G1, G2, G3 Gaussian distributions correspond to three different kinds of Fe sites in amorphous matrix, whereas the fourth one (G4), due to its average hyperfine induction value, can be attributed to the interface zone, i.e. to Fe sites exactly in the grain boundaries or in the amorphous matrix but in close contact with the grains [21].

The magnetic hyperfine distribution curves provide direct information relating to short-range order of the amorphous phase [14]. As can be realized in Fig. 6b, the formation of α-Fe phase affects the magnetic structure of the residual amorphous

[DOI: 10.22068/ijmse.16.3.1]

matrix. Each hump in the hyperfine field distribution curve (Fig.6b) represents distinct regions of resonant atoms with hyperfine interactions ranging from week magnetic fields (12-20 T) up to strong hyperfine magnetic field (25-30 T). The low field component can be attributed to the Fe atoms primarily B atoms as the nearest neighbors [22]. This statement could be confirmed by available data on FeB powders [22]. Rodrigues Torres et al. [22, 23] and Shinjo et al. [24] reported hyperfine fields of 10T and 12T for FeB, respectively.

As can be observed in Fig. 6a, annealing of the amorphous $Fe_{85.3}B_{11}P_3Cu_{0.7}$ ribbons at 440˚C for 10 minutes (sample 440-10) leads to the appearance of sharp and isolated lines in the Mossbauer spectrum which confirms the formation of nanocrystalline grains in the annealed ribbons. The best fitted hyperfine parameters for the sample 440-10 are listed in Table 2. In this table B_{cr}, IS_{cr} and QS_{cr} are the hyperfine magnetic field induction, the isomer shift and the quadrupole splitting of α-Fe crystalline phase, respectively and Γ_{FWHM} is the full width at half maximum of the lines of the sextet of α-Fe phase.

As can be seen in table 2, the sample contains 53% residual amorphous matrix and 47% α-Fe nanocrystalline phase. It is worth noticing that the average value of B_{hf} in the residual amorphous phase is somewhat higher than in the parent alloy (table 1 and 2), although the matrix becomes poorer in iron because of α-Fe crystallization.

With comparing the hyperfine field distributions for the amorphous and annealed samples (Figs. 3b, 6b), it can be realized that even though the amount of amorphous phase is falling, the number of Fe atoms which have mostly B and possibly some Cu atoms as their nearest neighbors is rising, as stated by Miglierini et. al [14]. Increasing the number of iron atoms surrounded by B and Cu atoms and their poor solubility in α-Fe phase leads to their clustering. Consequently, the standard deviation of hyperfine field distribution for the annealed sample is increased [14]. Miglierini [14] has proposed that the variations of local arrangement of the constituent elements in the residual amorphous matrix show itself by increasing the standard deviation. This indicates that during the annealing of an amorphous ribbon, not only the nanocrystalline phase is formed but also the residual amorphous matrix undergoes considerable changes [14].

In fact, chemical and topological changes in the short-range result in the formation of new surroundings for the resonant atoms; consequently, changes in the magnetic properties of the residual amorphous phase (reflected by the average hyperfine field values) and in the structure (reflected through the standard deviation) are revealed [14].

Further comparison of Fig. 6b with Fig. 3b reveals a decrease in the high field hump in the annealed sample, which suggest rather rapid crystallization in $Fe_{85.3}B_{11}P_3Cu_{0.7}$ ribbons. The high field hump represents those Fe atoms which have B and P atoms as the nearest neighbors and since these are the elements from which the nanocrystalline phases are formed, it is mainly high field hump which decreases during crystallization.

On the other hand, the average isomer shift has increased after annealing at 440 ˚C which confirms the decrease of electron density at the iron nucleus. This effect can be ascribed to the migration of some Fe atoms from the amorphous phase to form α-Fe nanocrystalline grains.

The transmission Mossbauer spectrum of the $Fe_{85.3}B_{11}P_3Cu_{0.7}$ ribbons annealed at 530 ˚C for 10 minutes is presented in Fig. 7 and was best fitted with four subspectra. One subspectrum with a hyperfine field of 33.2 T attributed to α-Fe phase and the others with hyperfine fields of 29.9, 27.3 and 23.2 T correspond to the three nonequivalent iron sites $Fe_I(8g)$, $Fe_{II}(8g)$ and $Fe_{III}(8g)$, in BCT Fe_3B, respectively [19], which is in agreement with XRD results.

The best fitted hyperfine parameters for the sample annealed at 530 ˚C are listed in Table 3. In this table B_{cr}, $IS_{cr,}$ and QS_{cr} are the hyperfine magnetic field induction, the isomer shift and the quadrupole splitting of a crystalline phase, respectively, and Γ_{FWHM} is the full width at half maximum of the characteristic lines of a crystalline phase. As can be understood from table 3, each of these three nonequivalent iron sites shows a small effective quadrupole interaction indicating that none of these sites has a cubic symmetry [19]. The hyperfine parameters for Fe_3B crystalline phase slightly differ from those reported by some other researchers [19, 25- 27]. It may be connected with the presence of elements other than Fe and B in-

[DOI: 10.22068/ijmse.16.3.1]

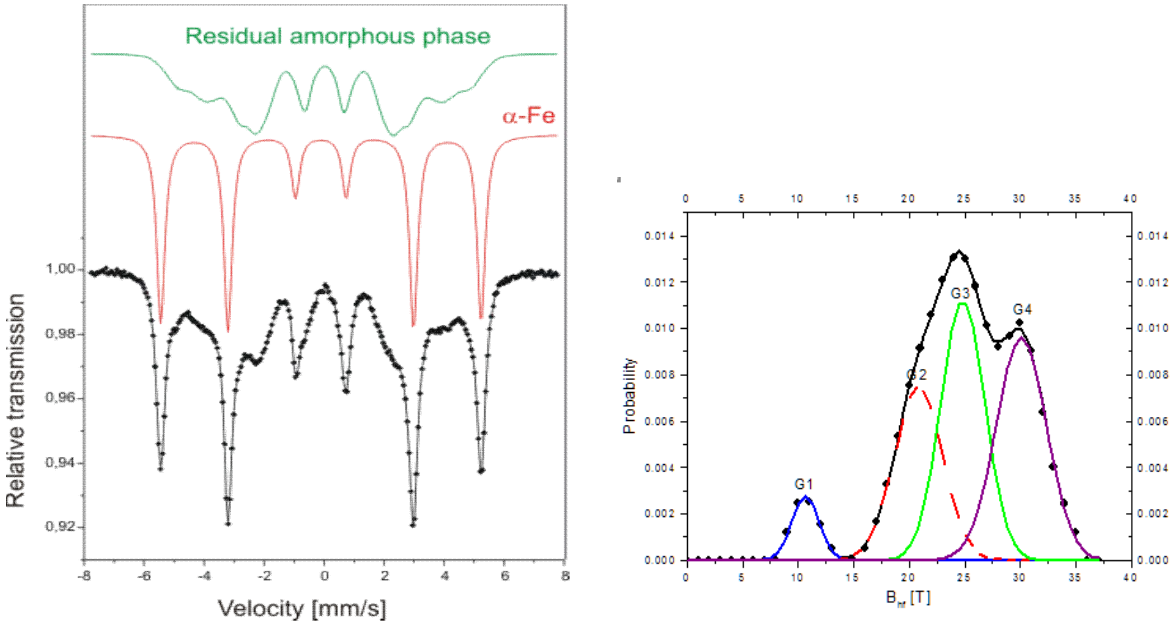

Fig. 6. Room temperature transmission Mossbauer spectrum (a) and corresponding hyperfine field distribution (b) of the $Fe_{85.3}B_{11}P_3Cu_{0.7}$ ribbons annealed at 440 ˚C for 10 minutes.

Table 2. Best fitted hyperfine parameters for the $Fe_{85.3}B_{11}P_3Cu_{0.7}$ ribbons annealed at 440 ˚C for 10 minutes.

Phase	$\overline{B_{hf}}$ [T]	ΔB_{hf} [T]	B_{cr} [T]	a [mm/(sT)]	b [mm/s]	$\overline{IS}$ [mm/s]	IS_{cr} [mm/s]	QS_{cr} [mm/s]	Γ_{FWHM} [mm/s]	$I_{2,5}$	A [%]
RAP*	24.88	5.29		-0.0011	0.04	0.12					53
α-Fe			33.115				-0.001	0.005	0.324	3.12	47

*RAP: Residual Amorphous Phase

corporated in the lattice.

Fe and B atoms can form various kinds of Fe-B compounds such as o-FeB, bct-Fe_2B, bct-Fe_3B, o-Fe_3B and fcc-$Fe_{23}B_6$ [20]. The structural and hyperfine field parameters for the different Fe-B compounds are reported by Zhang et al. [20]. Among these compounds, only FeB and Fe_2B are stable [20]. o-Fe_3B phase is structurally similar to Fe_3C in which each unit cell composed of two non-equivalent Fe sites, i.e. Fe(8g) and Fe(4c), and a single B site with a population ratio of 1: 2 [20].

The bct-Fe_3B is structurally similar to tetragonal Fe_3P in which each unit cell composed of 8 formula units [20]. This phase consists of three crystallographically non-equivalent Fe sites, i.e. $Fe_I(8g)$, $Fe_{II}(8g)$, $Fe_{III}(8g)$, with the same population having 2, 3, 4 metalloids nearest neighbors, respectively, and a single B site [20]. The reported hyperfine field and isomer shift values for the iron sites, I, II, III, by Le Caer et al. [25] are 28.7, 26.7, 22.5 T and 0.08, 0.04, 0.12 mm/s, respectively [20, 25].

In the bct-Fe_3B structure, the B atoms are lo-

[DOI: 10.22068/ijmse.16.3.1]

cated in the center of the trigonal prism formed by 6 nearest Fe atoms, i.e. 2 Fe_I(8g), 2 Fe_{II}(8g) and 2 Fe_{III}(8g), at the vertices; three other iron atoms are located at a slightly longer distance and bounded to each B atoms through a rectangular prism face (Fig. 8) [20, 26].

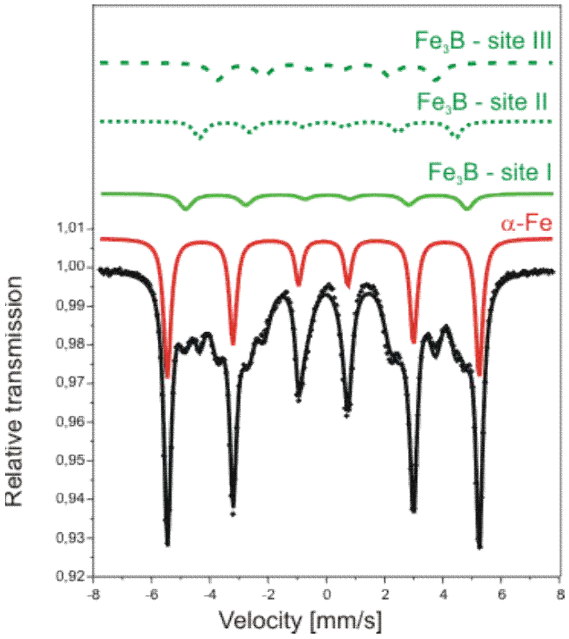

Fig. 7. Room temperature transmission Mossbauer spectrum for the $Fe_{85.3}B_{11}P_3Cu_{0.7}$ ribbons annealed at 530 ˚C for 10 minutes.

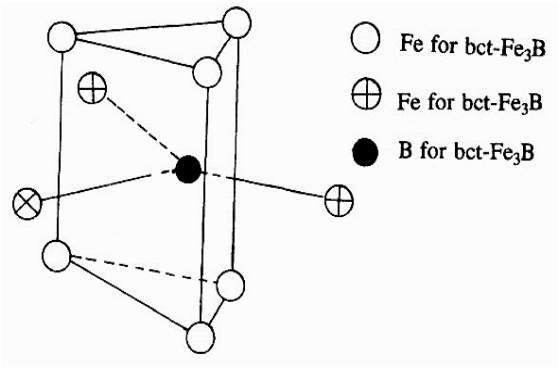

Fig. 8. The trigonal prism of bct-Fe_3B phase [26].

3.2. Magnetic Properties

In order to study the effect of the structural changes on the soft magnetic properties of rapidly solidified $Fe_{85.3}B_{11}P_3Cu_{0.7}$ ribbons during the annealing process, the room temperature hysteresis loops of the amorphous and annealed ribbons were measured by AGFM at room temperature. The curves corresponding to the amorphous ribbons and annealed samples at 440, 530 and 650 ˚C for 10 minutes are presented in Fig. 9 and the resulting magnetic properties are listed in table 4. In the inset, the evolution of the coercive field as a function of annealing temperature is shown.

Table 3. Best fitted hyperfine parameters for the $Fe_{85.3}B_{11}P_3Cu_{0.7}$ ribbons annealed at 530 ˚C for 10 minutes.

Phase	B_{cr} [T]	IS_{cr} [mm/s]	QS_{cr} [mm/s]	Γ_{FWHM} [mm/s]	$I_{2,5}$	[%]
α-Fe	33.196	-0.0005	-0.002	0.290	2.27	47
Fe_3B – site I	29.95	0.096	-0.031	0.54	2.17	18
Fe_3B – site II	27.27	0.087	0.121	0.46	1.95	13
Fe_3B – site III	23.18	0.113	-0.009	0.57	2.38	22

Table 4. Magnetic properties of the amorphous and annealed $Fe_{85.3}B_{11}P_3Cu_{0.7}$ ribbons at room temperature.

Annealing Temperature (˚C)	Magnetic Properties			
	H_c (Oe)	H_c (A/m)	M_s (emu/g)	M_s (T)
as-spun	0.3	24	187	1.79
440	0.7	56	220	2.11
530	14.2	1130	224	2.15
650	41.5	3302	202	1.94

[DOI: 10.22068/ijmse.16.3.1]

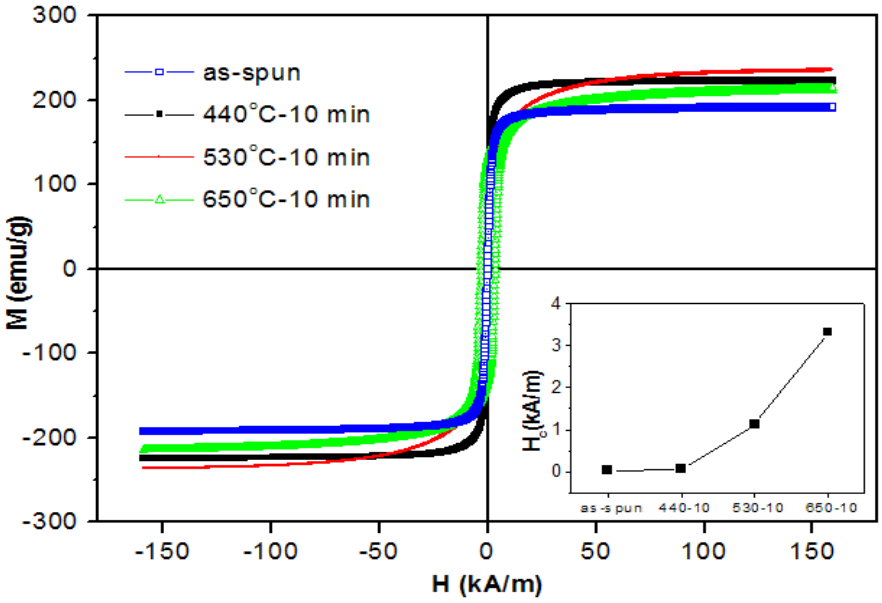

Fig. 9. Hysteresis loops at room temperature for the amorphous $Fe_{85.3}B_{11}P_3Cu_{0.7}$ ribbons annealed at 440, 530 and 650 ˚C for 10 minutes.

The results show that the saturation magnetization significantly increased after 10 minutes annealing at 440 ˚C. This may be attributed to the stress relieve in the residual amorphous phase and the increment of the volume fraction of α-Fe nanocrystals which are exchange coupled [28]. On the other hand, as shown in table 4 and in the inset of Fig. 9, the coercivity considerably increased with increasing the annealing temperature to 530 and 650 ˚C. This can be ascribed to the formation of bct-Fe_3B phase from the amorphous matrix. Herzer [29] investigated the anisotropy contributions in nanocrystalline Fe-based alloys and found that the soft magnetic properties can be significantly affected by the precipitation of small fractions of boride compounds like Fe_2B or Fe_3B due to their huge magnetocrystalline anisotropy. The magnetocrystalline anisotropy of Fe_2B and Fe_3B phases are 430 and -320 kJ/m^3, respectively [28].

It has been shown [16] that for suppressing the magnetocrystalline anisotropy, the randomly oriented grains should be coupled by exchange interaction. As a result, if the exchange interaction is reduced, the soft magnetic properties will degrade [16]. It has been proved [16] that the exchange coupling between the nanocrystalline grains takes place through the residual interfacial amorphous phase by which the nanocrystallites are surrounded. As a consequence, with increasing annealing temperature giving rise to the grain growth as well as the formation of boride compounds from the amorphous matrix, the amount of the residual amorphous phase and consequently the exchange interaction between the nanocrystallites is drastically reduced. This causes a significant increase in coercivity with increasing the annealing temperature.

4. CONCLUSIONS

In the present work, the microstructure and soft magnetic properties for the as-spun and annealed Fe-rich $Fe_{85.3}B_{11}P_3Cu_{0.7}$ ribbons were studied and the results are summarized as follows:

1. The XRD results revealed that the α-Fe crystalline phase is probably present on the surfaces of rapidly quenched ribbons while the Mossbauer results confirmed the achievement of completely amorphous structure for the volume of the sample.
2. The hyperfine field distribution for the as-spun and annealed ribbons at 440 ˚C showed two separated components suggesting the presence of two structurally and magnetically

[DOI: 10.22068/ijmse.16.3.1]

distinct surroundings for the iron atoms. The low field components can be attributed to those Fe atoms which have primarily Cu and B as nearest neighbors whereas the high field components are ascribed to the Fe atoms surrounded by P and B atoms.

3. The magnetic hyperfine distribution curves indicated that the formation of α-Fe phase affects the magnetic structure of the residual amorphous matrix.
4. The variation of α-Fe crystallite size at different temperatures showed that the presence of the residual amorphous matrix can hinder the grain growth.
5. Annealing the as-spun ribbons for 10 minutes at 440 ˚C results in a significant increase in saturation magnetization (220 emu/g) which makes them good candidates for electrical power applications.

REFERENCES

1. Herzer, G., "Soft magnetic nanocrystalline materials", Scr. Metall. Mater., 1995, 3, 1741-1756.
2. Yoshizawa, Y., Oguma, S., Yamauchi, K., "New Fe-based soft magnetic alloys composed of ultrafine grain structure", J. Appl. Phys., 1988, 64, 6044-6046.
3. Makino, A., Men, H., Kubota, T., Yubuta, K. and Inoue, A., "FeSiBPCu Nanocrystalline Soft Magnetic Alloys with High Bs of 1.9 Tesla Produced by Crystallizing Hetero-Amorphous Phase", Mater. Trans., 2009, 50, 204-209.
4. Cao, C. C., Wang, Y. G., Zhu, L., Meng, Y., Dai, Y. D. and Chen, J. K., "Evolution of structural and magnetic properties of the FeCuBP amorphous alloy during annealing", J. Alloys Compd., 2017, 722, 394-399.
5. Kong, F., Wang, A., Fan, X., Men, H. and Shen, B., "High Bs $Fe_{84-x}Si_4B_8P_4Cu_x$ (x= 0–1.5) nanocrystalline alloys with excellent magnetic softness", J. Appl. Phys., 2011, 109 (7), 07A303.
6. Lashgari, H. R., Chu, D., Xie, S., Sun, H., Ferry, M. and Li, S., "Composition dependence of the microstructure and soft magnetic properties of Fe-based amorphous/nanocrystalline alloys: A review study", J. Non-Cryst. Solids, 2014, 391, 61-82.
7. Makino, A., Men, H., Kubota, T., Yubuta, K., Inoue, A., "New Fe-metalloids based nanocrystalline alloys with high BS of 1.9T and excellent magnetic softness", J. Appl. Phys., 2009, 105, 07A308.
8. Brand, R. A., "Improving the validity of hyperfine field distributions from magnetic alloys", Nucl. Instrum. Methods Phys. Res. B, 1987, 28, 398-416.
9. Kraus, L., Zivotský, O., Postava, K., Svec, P. and Janickovic, D., "Exchange Bias in Surface-Crystalline Fe-Nb-B Ribbons", IEEE Trans. Magn., 2008, 44, 3875-3878.
10. Vishwanadh, B., Balasubramaniam, R., Srivastava, D. and Dey, G. K., "Effect of Surface Morphology on Atmospheric Corrosion Behaviour of Fe-based Metallic Glass, $Fe_{67}Co_{18}Si_{14}B_1$", Bull. Mater. Sci., 2008, 31, 693–698.
11. Saad, Y., Hidouri, M., Álvarez-Serrano, I., Veiga, M. L., Wattiaux, A., Amara, Mongi B., "Crystal structure and Mössbauer spectroscopy of a new iron phosphate $Mg_{2.88}Fe_{4.12}(PO_4)_6$", J. Alloys Compd., 2014, 584, 625–630.
12. Bensebaa, N., Alleg, S., Greneche, J. M., "Phase transformations of mechanically alloyed Fe–Cr–P–C powders", J. Alloys Compd., 2005, 393, 194–203.
13. Pietrusiewicz, P., Nabiałek, M., Dospiał, M., Gruszka, K., Błoch, K., Gondro, J., Bragiel, P., Szota, M., Stradomski, Z., "Influence of production method on the magnetic parameters and structure of $Fe_{61}Co_{10}Y_8Nb_1B_{20}$ amorphous alloys in the as-quenched state", J. Alloys Compd., 2014, 615, S67-S70.
14. Miglierini, M., "Mossbauer-effect study of the hyperfine field distributions in the residual amorphous phase of Fe-Cu-Nb-Si-B nanocrystalline alloys", J. Phys.: Condens. Matter, 1994, 6, 1431-1438.
15. Jafari, S., Beitollahi, A., Eftekhari Yekta, B., Ohkubo, T., Budinsky, V., Marsilius, M., Herzer, G., and Hono, K., "Atom Probe Analysis and Magnetic Properties of Nanocrystalline $Fe_{84.3}Si_4B_8P_3Cu_{0.7}$", J. Alloys Compd., 2016, 674, 136-144.
16. Herzer, G., "Nanocrystalline Soft Magnetic Alloys, in: Handbook of Magnetic Materials", ed. K.H.J. Buschow, vol. 10, Elsevier, Amsterdam, 1997.pages?
17. Jia, Y. Y., Wang, Z., Shi, R. M., Yang, J., Kang, H. J., and Lin, T., "Influence of Ni Addition on Structure and Magnetic Properties of FeCo-based Finemet Type Alloys", J. Appl. Phys., 2011, 109, 073917.
18. Agudo, P. and Vázquez, M., "Influence of Ni on the Structural and Magnetic Properties of $Ni_xFe_{73.5-x}Si_{13.5}B_9Nb_3Cu_1$ ($0 \le x \le 25$) alloys", J. Appl. Phys., 2005, 97, 023901-6.
19. Cheng, Z. H., Shen, B. G., Mao, M. X., Sun, J. J., Wang, F. W., Li, F. S. and Zhang, Y. D., "The development of the phase composition in melt-

[DOI: 10.22068/ijmse.16.3.1]

spun $Gd_4Fe_{77.5}B_{18.5}$ alloys with thermal treatment: a combined NMR and Mossbauer study", J. Phys. D: Appl. Phys., 1997, 30, 2812–2817.
20. Zhang, Y. D., Budnick, J. I., Ford, J. C. and Hines, W. A., "Some applications of NMR to the study of magnetically-ordered materials with emphasis on the short-range order in (Fe-B)-based crystalline and amorphous alloys", J. Magn. Magn. Mater., 1991, 100, 13-37.
21. Miglierini, M. and Greneche, J. M., "Mossbauer spectrometry of Fe(Cu)MB-type nanocrystalline alloys: I. The fitting model for the Mossbauer spectra", J. Phys.: Condensed Matter, 1997, 9, 2303–2319.
22. Jartych, E., Pekala, K., Jaskiewicz, P., Latuch, J., Pekala, M., Grabski, J., "Structural and magnetic properties of bulk amorphous alloys Fe–Al–Ga–P–B–Si", J. Alloys Compd., 2002, 343, 211–216.
23. Torres, C. R., Sanchez, F. H., Zelis, L. M. and Fernandez van Raap, M. B., "Mechanical Grinding of Iron Borides", Mater. Sci. Forum, 1995, 179-181, 103-108.
24. Shinjo, T., Itoh, F., Takaki, H., Nakamura, Y. and Shikazono, N., "Fe^{57} Mossbauer Effect in Fe_2B, FeB and Fe_3C", J. Phys. Soc. Jpn, 1964, 19, 1252-1252.
25. Caer, G. Le and Durois, J. M., "About the asymmetries in Mössbauer spectra of magnetic amorphous transition metal—metalloid alloys", Phys. Status Solidi A, 1981, 64, 275-282.
26. Cheng, Z. H., Shen, B. G., Mao, M. X., Sun, J. J., Zhang, Y. D. and Li, F. S., Magnetism, "phase composition, and hyperfine fields of melt-spun Nd-Fe-8 alloys with a few percent of neodymium, Phys." Rev. B, 1995, 52, 9427-9436.
27. Hinomura, T., Nasu, S., Kanekiyo, H. and Hirosawa, S., "Magnetic Properties of Nd-Fe-B Nanocrystalline Composite Magnets", J. Jpn. Inst. Met., 1997, 61, 184-190.
28. Manjura Hoque, S., Liba, S. I., Anirban, A., Choudhury, "Shamima and Akhter, Shireen, Ultra-soft magnetic properties and correlated phase analysis by 57Fe Mössbauer spectroscopy of $Fe_{74}Cu_{0.8}Nb_{2.7}Si_{15.5}B_7$ alloy", AIP Adv., 2016, 6, 025304.
29. Herzer, G., "Anisotropies in Soft Magnetic Nanocrystalline Alloys", J. Magn. Magn. Mater, 2005, 294, 99–106.

[DOI: 10.22068/ijmse.16.3.1]